Strain Accumulation Rates in the Western United States Between 1970 and 1978

W. H. PRESCOTT,[1] J. C. SAVAGE, AND W. T. KINOSHITA

U.S. Geological Survey, Menlo Park, California 94025

The rate of dilatation and the rate and direction of shear have been determined from trilateration data for 23 Geodolite networks in the western United States. Sixteen nets are located along the San Andreas fault system between Point Reyes, California, and the United States–Mexico border. Other locations are across the Garlock fault in California; across Puget Sound near Seattle, Washington; near Hanford in eastern Washington; near Hebgen Lake in Montana; across the Wasatch fault at Ogden, Utah; across the Rio Grande rift at Socorro, New Mexico; and Dixie Valley in Nevada; and at the northern end of Owens Valley on the California-Nevada border. Implicit in the treatment are the assumptions that the strain was accumulating at a constant rate over the time period (within the interval 1970–1978) and over the local area (usually about 50-km diameter) covered by the surveys. Of the nets located away from the San Andreas fault, only Ogden and Hebgen show significant strain accumulation. At Ogden the deformation is principally an east-west compression of 0.23 ± 0.05 μstrain/yr and at Hebgen Lake a northeast-southwest extension of 0.17 ± 0.03 μstrain/yr. Along the San Andreas fault system the rate of shear is 0.2 to 0.4 μstrain/yr. The direction of shear agrees very well with the surface strike of nearby faults. This agreement is maintained even in regions like the 'big bend,' where both the fault strike and the observed shear direction are more westerly than they are elsewhere. Shear strain in northern California appears to be concentrated more closely on the faults, whereas in southern California the strain is a broader, smoother feature. In the San Francisco Bay area the strain data indicate slip at depth on both the San Andreas and the Calaveras faults. In addition to the observed shear the nets in California indicate a negative dilatation (areal decrease) of about 0.2 μstrain/yr. This dilatation is unexplained, but the following sources appear unlikely: (1) systematic survey error, (2) an association with the southern California uplift, (3) an association with the big bend in the San Andreas fault in Southern California, or (4) the result of the superposition of a uniaxial strain on the Pacific–North American plate boundary shear.

INTRODUCTION

As part of the earthquake studies program of the U.S. Geological Survey a large number of distances have been measured very precisely several times during the interval 1970–1978. These measurements, which are concentrated in regions of appreciable seismic risk, constitute a measure of deformation that presumably is related to the earthquake process. In this paper we present a summary of the data by reporting average rates of strain accumulation in the various seismic regions. A typical rate of strain accumulation is found to be of the order of 0.1 μstrain/yr tensor strain.

To detect such low rates of deformation with present distance-measuring instruments requires averaging a number of observations and/or looking at time periods over which strain changes are large in relation to the noise level. In this study, about 3000 observations of distance, spanning the period from 1970 to early 1978, were included. The data naturally divide into 23 geographic sections henceforth referred to as Geodolite networks or nets. Fifteen networks are along the San Andreas fault system; other nets are located across the Garlock fault in California; across Puget Sound near Seattle, Washington; near Hanford in eastern Washington; near Hebgen Lake in Montana; across the Wasatch fault at Ogden, Utah; across the Rio Grande rift at Socorro, New Mexico; along Dixie Valley in Nevada; and at the northern end of Owens Valley on the California-Nevada border. Each survey of a net is generally carried out within the span of a few weeks. Each net covers an area of radius between 10 and 50 km, includes between 10 and 60 individual lines, and has been surveyed between 2 and 8 times. To extract strain rates from the noise, we have made two assumptions about the nature of the strain accumulation. First, we have assumed that spatially, the strain accumulates uniformly over each network. This is probably a simplification of the actual mode of strain accumulation. Each net spans a considerable area, and the strain might vary appreciably within that area. The strains we obtain are averages over the area involved. In some cases the average is not very meaningful, and we have tried to exclude such cases. For example, between San Juan Bautista and Cholame in central California, deformation occurs principally as slip on the fault. Consequently, strain is not uniform over any area that crosses the fault. We have therefore excluded data from this area except for some lines near the northern end of the creeping section, lines that do not cross known creeping faults. In other areas, deviations from spatial uniformity are probably within the uncertainties in the observations. The second assumption is that the rate of strain accumulation is constant. That is, for each network we assume that in any given time period, say, between January 1970 and January 1973, the change in strain is the same as during any other time period of the same length. Since all of the observations span only an 8-year period and in some nets much less, this is a reasonable first approximation. Data from the U.S. Atomic Energy Commission's Nevada Test Site [*Savage et al.*, 1974], where strain is largely imposed by nuclear explosions, clearly violate this assumption and are not considered here.

Because all of the different nets span different time periods, it is convenient to discuss strain rates rather than strains that require specifying a time period and are difficult to compare. All strains given in this paper will be in annual rates, as indicated by a dot over the strain symbol. Strain rates were extracted from the observations by the method of least

[1] Also at Rock Physics Project, Stanford University, Stanford, California 94305.

Paper number 9B0527.

squares. The method used is similar to that described by *Prescott* [1976] for triangulation data.

OBSERVATIONS

The data used in this study were observations of distance made by the U.S. Geological Survey (USGS) between 1970 and 1978. In one area, observations made by the California Division of Mines and Geology (CDMG) were included. All lengths were observed with electro-optical distance-measuring instruments using airborne meteorological sensors flown along the line at the time of ranging to determine the refractivity of the atmosphere. Details of the measuring techniques and precision obtained by the USGS were described by *Savage and Prescott* [1973]. The CDMG used similar techniques, and those observations should have a similar precision. The precision of the observations is summarized in Figure 1; clearly, the precision in strain is much greater on the longer lines.

Assume that we have a set of length observations and the times of observation L_{ij}, T_{ij}, where $i = 1, \cdots, n$ identifies the line and $j = 1, \cdots, n_i$ identifies the observations of the ith line. By definition, the strain in the ith line at time T_{ij} is

$$\epsilon_i = (L_{ij} - L_i)/L_i \tag{1}$$

where L_i is the unknown length at time T_i and

$$T_i = \left(\sum_{j=1}^{n_i} T_{ij}\right) \Big/ n_i$$

Since $L_{ij} - L_i \ll L_i$, we can replace L_i in the denominator of (1) by L_{i1} (or any other of the observed lengths). Also (1) can be converted to a strain rate by dividing by $(T_{ij} - T_i)$; thence

$$\dot{\epsilon}_i = (L_{ij} - L_i)/[L_{i1}(T_{ij} - T_i)] \tag{2}$$

Since the strain field is uniform, $\dot{\epsilon}$ can be expressed as a function of the azimuth θ and the strain rate components $\dot{E}_{11}$, $\dot{E}_{12}$, and $\dot{E}_{22}$, where $\dot{E}_{11}$ is the extension rate in the east-west direction, $\dot{E}_{22}$ the extension rate in the north-south direction, and $\dot{E}_{12}$ the right lateral shear across an east-west line (see, for example, *Jaeger and Cook* [1969, p. 39]):

$$\dot{\epsilon}_i = \dot{E}_{11} \sin^2 \theta_i + \dot{E}_{12} \sin 2\theta_i + \dot{E}_{22} \cos^2 \theta_i \tag{3}$$

Combining (2) and (3) and rearranging, we have

$$L_{ij} = L_i + L_{i1}(T_{ij} - T_i)(\dot{E}_{11} \sin^2 \theta_i + \dot{E}_{12} \sin 2\theta_i + \dot{E}_{22} \cos^2 \theta_i) \tag{4}$$

In (4), L_{i1} and θ_i are constant for any particular line; L_{ij} and $T_{ij} - T_i$ refer to a particular observation; and L_i, $\dot{E}_{11}$, $\dot{E}_{12}$, and $\dot{E}_{22}$ are unknowns. Equation (4) is an observation equation,

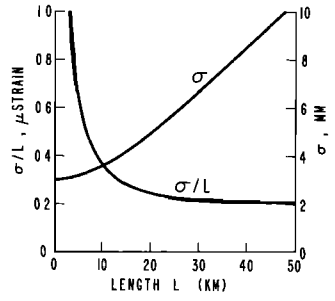

Fig. 1. Plot of standard deviation in a single observation of a distance measured by the techniques described in the text. Standard deviation is shown both in millimeters (right vertical axis) and in strain units (left vertical axis).

and the set of all such observations equations can be solved by standard least squares procedures to obtain estimates of $\dot{E}_{11}$, $\dot{E}_{12}$, $\dot{E}_{22}$, and the L_i. Because of the choice of T_i, L_i can be evaluated independently of the strain components:

$$L_i + \left(\sum_{j=1}^{n_i} L_{ij}\right) \Big/ n_i \tag{5}$$

Thus solving for $\dot{E}_{11}$, $\dot{E}_{12}$, and $\dot{E}_{22}$ requires inverting only a 3×3 matrix.

All of the observations of lines in one net were combined for a single least squares determination of the strain field, given in Table 1. A number of nets were excessively noisy. These nets, all of which had standard deviations in excess of 0.2 μstrain/yr, were located near Libby, Montana (one); near Orofino, Idaho (one); two at the Nevada Test Site; and three near the San Andreas fault on the San Francisco Peninsula. The three nets along the San Andreas fault had large uncertainties because of their small aperture; the Libby net had a large standard deviation because of the short time period spanned by the observations; and Orofino was ill determined for both of these reasons. The large standard deviations at the Nevada Test Site are a reflection of the temporal inhomogeneity in the strain field. Whatever the reasons for the large standard deviations, all nets with standard deviations in $\dot{E}_{11}$, $\dot{E}_{12}$, and $\dot{E}_{22}$ exceeding 0.2 μstrain/yr were excluded from this analysis. Strain rates at the remaining nets are shown in Figures 2, 3, and 4.

NOTATION

The notation used in discussing horizontal strain in this paper is defined below. For all symbols except $\dot{\gamma}_1'$ and $\dot{\gamma}_2'$ the x_1 axis is directed east, and the x_2 axis is directed north. The angles ϕ and ψ are measured clockwise from the x_2 axis; that is, they represent azimuth measured clockwise from north:

- $\dot{E}_{11}$ rate of change of length per unit length in the direction of the x_1 axis (a tensor component), positive for extension;
- $\dot{E}_{12}$ rate of tensor shear across any line parallel to the x_1 axis (a tensor component), positive for right lateral shear;
- $\dot{E}_{22}$ rate of change of length per unit length in the direction of the x_2 axis (a tensor component), positive for extension;
- $\dot{\gamma}_1$ rate of engineering shear across any line parallel to the line $x_2 = -x_1$ (not a tensor component), positive for right lateral shear, equal to $\dot{E}_{11} - \dot{E}_{22}$;
- $\dot{\gamma}_2$ rate of engineering shear across any line parallel to the x_1 axis (not a tensor component), positive for right lateral shear, equal to $2\dot{E}_{12}$;
- $\dot{\Delta}$ rate of dilatation or change in area per unit area, positive for increase in area, equal to $\dot{E}_{11} + \dot{E}_{22}$ (note: this symbol has also been used to denote mean radial dilation [cf. *Frank*, 1966], which is equal to one-half the areal dilatation used here);
- $\dot{\gamma}$ rate of engineering shear across that direction having the highest shear rate (not a tensor component), always greater than zero, also referred to as total shear;
- ψ azimuth of the line across which right lateral shear is maximum, convenient to give the corresponding bearing rather than the azimuth, but for any formal use of ψ (as in the formulas following this notation) the azimuth must be used;
- $\dot{\epsilon}_1$ maximum principal strain rate, rate of change of length per unit length in that direction having the algebraically greatest extension rate (a tensor component), extension positive;

TABLE 1. Strain Rate Components Obtained by Least Squares Adjustment of Trilateration Data

Net Name	Location	$\dot{E}_{11}$, μstrain/yr	$\dot{E}_{12}$, μstrain/yr	$\dot{E}_{22}$, μstrain/yr
Anza	S. California	−0.04 ± 0.02	0.01 ± 0.02	−0.27 ± 0.03
Bay	N. California	0.11 ± 0.02	−0.14 ± 0.02	−0.27 ± 0.01
(Black Mountain)	N. California	0.28 ± 0.22	0.35 ± 0.26	−0.25 ± 0.28
Cajon	S. California	0.03 ± 0.07	0.01 ± 0.07	0.37 ± 0.07
Excelsior	W. Nevada	0.02 ± 0.03	−0.02 ± 0.02	−0.04 ± 0.02
Fallon	W. Nevada	0.04 ± 0.07	0.02 ± 0.05	−0.05 ± 0.06
Garlock	S. California	−0.03 ± 0.02	−0.05 ± 0.02	−0.15 ± 0.04
Gavilan	N. California	−0.06 ± 0.10	−0.09 ± 0.07	−0.18 ± 0.08
Geyser	N. California	0.15 ± 0.03	−0.11 ± 0.03	−0.28 ± 0.03
Hanford	S. Washington	−0.05 ± 0.02	−0.02 ± 0.01	−0.05 ± 0.02
Hebgen	S. Montana	−0.04 ± 0.03	0.07 ± 0.02	0.14 ± 0.03
Hollis	N. California	0.16 ± 0.03	0.08 ± 0.02	−0.11 ± 0.03
(Libby)	W. Montana	−0.53 ± 0.31	0.35 ± 0.24	−0.21 ± 0.28
Los Padres	S. California	−0.02 ± 0.02	−0.01 ± 0.02	−0.25 ± 0.02
(Lake San Andreas)	N. California	0.47 ± 0.29	0.18 ± 0.27	−1.10 ± 0.31
Mocho	N. California	−0.18 ± 0.04	−0.06 ± 0.03	−0.14 ± 0.04
Napa	N. California	−0.08 ± 0.02	−0.08 ± 0.02	−0.13 ± 0.02
(Nevada Test Site)	S.W. Nevada	−1.22 ± 0.23	0.10 ± 0.24	−0.99 ± 0.33
Ogden	E. Utah	−0.16 ± 0.02	−0.02 ± 0.02	−0.08 ± 0.02
(Orofino)	W. Idaho	−0.14 ± 0.31	0.67 ± 0.34	−1.14 ± 0.42
Pajaro	N. California	−0.04 ± 0.04	0.02 ± 0.04	−0.30 ± 0.05
Palmdale	S. California	0.07 ± 0.03	0.07 ± 0.02	−0.24 ± 0.03
Point Reyes	N. California	0.19 ± 0.15	−0.12 ± 0.09	−0.50 ± 0.20
(Radio Facility)	N. California	0.40 ± 0.22	−0.25 ± 0.22	−0.48 ± 0.30
Salton	S. California	0.04 ± 0.01	0.01 ± 0.01	−0.31 ± 0.02
San Fernando	S. California	−0.02 ± 0.03	−0.07 ± 0.03	−0.41 ± 0.05
Santa Rosa	N. California	0.17 ± 0.06	−0.01 ± 0.05	−0.16 ± 0.08
Seattle	N.W. Washington	−0.09 ± 0.03	−0.06 ± 0.03	0.01 ± 0.05
Socorro	Cen. New Mexico	−0.05 ± 0.02	−0.00 ± 0.02	−0.09 ± 0.03
Tehachapi	S. California	−0.00 ± 0.02	0.06 ± 0.02	−0.24 ± 0.02
(Yucca)	S.W. Nevada	−0.56 ± 0.26	−0.08 ± 0.18	−0.00 ± 0.21

$\dot{E}_{11}$ measures E-W extension, $\dot{E}_{22}$ N-S extension, and $\dot{E}_{12}$ right lateral tensor shear across an E-W line or left lateral shear across a N-S line. Parentheses indicate regions with excessive standard deviations which are not examined further.

$\dot{\epsilon}_2$ minimum principal strain rate, rate of change of line length per unit length in that direction having the algebraically smallest extension rate (a tensor component), positive for extension;

ϕ azimuth of direction of maximum principal strain rate;

$\dot{\gamma}_1'$ same as $\dot{\gamma}_1$ except in a coordinate system oriented with the x_1 axis parallel to the strike of the fault;

$\dot{\gamma}_2'$ same as $\dot{\gamma}_2$ except in a coordinate system oriented with x_2 axis parallel to the strike of the fault;

β azimuth of the horizontal normal to the local strike of

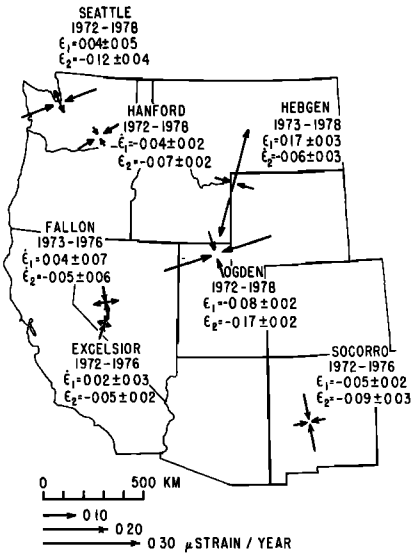

Fig. 2. Map indicating location of strain-field determinations in western United States. Those in California are not shown. Parameter $\dot{\epsilon}_1$ is the algebraically larger principal strain rate, and $\dot{\epsilon}_2$ the smaller, extension reckoned positive. Position of the net is at the center of the arrows, and orientation of the strain field is indicated by the orientation of the arrows.

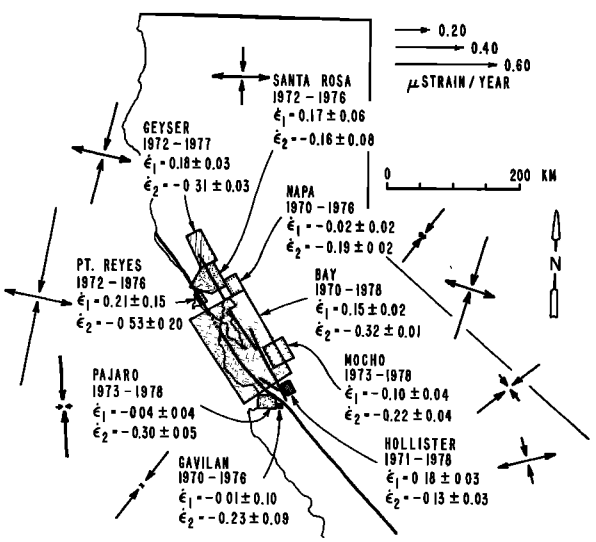

Fig. 3. Map indicating location of strain field determinations in northern California. Parameter $\dot{\epsilon}_1$ is the algebraically larger principal strain rate, and $\dot{\epsilon}_2$ the smaller, extension reckoned positive. Orientation of strain field indicated by the orientation of the arrows. Area covered by each net is indicated by shading. Trace of major faults is also shown.

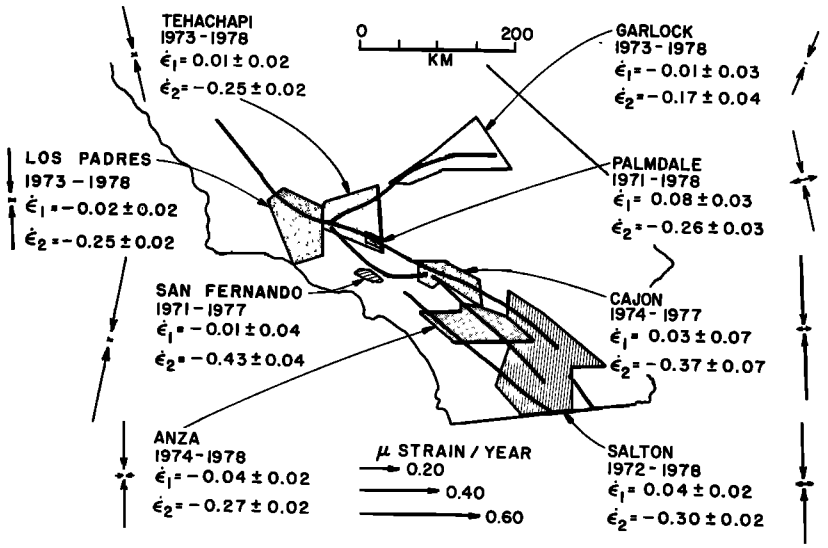

Fig. 4. Map indicating location of strain field determinations in Southern California. Parameter $\dot{\epsilon}_1$ is the algebraically larger principal strain, and $\dot{\epsilon}_2$ the smaller, extension reckoned positive. Orientation of strain field indicated by orientation of the arrows. Area covered by each net is indicated by shading. Trace of major faults is also shown.

the fault, thus the clockwise angle required to rotate a coordinate system with the x_1 axis directed east into one with the x_1 axis directed parallel to the local strike of the fault.

Note that $\dot{\gamma}_1'$ and $\dot{\gamma}_2'$ as used by *Thatcher* [1975*a*, *b*] refer to a coordinate system oriented with the x_1 axis 45° counterclockwise to the local fault strike. In *Thatcher*'s [1975*a*, *b*] notation, shear across a line parallel to the local strike of the fault is given by $\dot{\gamma}_1'$, whereas in our notation it is given by $\dot{\gamma}_2'$. Relations among the various quantities are given in the following equations. All uncertainties are given as ±1 standard deviation. All strain rates are given in units of microstrains per year (1 ppm/yr).

$$\dot{\gamma}_1 = \dot{E}_{11} - \dot{E}_{22}$$
$$\dot{\gamma}_2 = 2\dot{E}_{12}$$
$$\dot{\Delta} = \dot{E}_{11} + \dot{E}_{22}$$
$$\dot{\gamma} = (\dot{\gamma}_1^2 + \dot{\gamma}_2^2)^{1/2}$$
$$\psi = \tfrac{1}{2} \arctan (-\dot{\gamma}_1/\dot{\gamma}_2)$$
$$\dot{\epsilon}_1 = \tfrac{1}{2}(\dot{\Delta} + \dot{\gamma})$$
$$\dot{\epsilon}_2 = \tfrac{1}{2}(\dot{\Delta} - \dot{\gamma})$$
$$\phi = \tfrac{1}{2} \arctan (\dot{\gamma}_2/-\dot{\gamma}_1) = \psi - 45$$
$$\dot{\gamma}_1' = \dot{\gamma}_1 \cos 2\beta - \dot{\gamma}_2 \sin 2\beta$$
$$\dot{\gamma}_2' = \dot{\gamma}_1 \sin 2\beta + \dot{\gamma}_2 \cos 2\beta$$

Western United States

Strain fields have been determined for two nets in Washington, one in Montana, one in Utah, one in New Mexico, and two in Nevada. The principal strain components for these seven areas are shown in Figure 2. Although the noise level is less than 0.1 μstrain/yr, most of the strain rates are statistically insignificant; that is, most rates do not differ from zero at the 95% confidence level. This is an interesting result because with the exception of the Hanford net in eastern Washington, all of these nets are located in seismically active areas. In particular, the two nets in Nevada, Fallon and Excelsior, have been the site of a number of moderate earthquakes during this century. Larger earthquakes in this region were the 1932 Cedar Mountain earthquake (M = 7.3) and the 1954 Dixie Valley–Fairview Peak earthquake (M = 7.1). In spite of this considerable seismicity, some of it accompanied by surface rupture, the strain rate for both of these nets over the period 1973–1976 was less than 0.1 μstrain/yr.

The nets located near Hanford on the Columbia River in eastern Washington and across Puget Sound at Seattle both indicate strain accumulation rates of the order of 0.1 μstrain/yr. Only the dilatational component is significant. The three nets farther east indicate significant rates of deformation. Near Hebgen Lake in southwest Montana, the trilateration data indicate northeast-southwest extension at a rate of $\dot{\epsilon}_1 = 0.17 \pm 0.03$ μstrain/yr. The Hebgen net spans the rupture associated with the 1959 Hebgen Lake earthquake. This M = 7.1 earthquake was accompanied by as much as 7 m of subsidence, and an area in excess of 200 km² subsided more than 3 m [*Myers and Hamilton*, 1964]. A nodal plane solution [*Ryall*, 1962] indicated that the earthquake was a result of normal slip on a fault plane which strikes N80°W ± 10° and dips 54°SW ± 8°, a solution consistent with the observed surface faulting. Our observations of N-S extension with an azimuth of N19°E ± 5° indicate continued deformation in the sense and direction that caused the earthquake. The difference between the direction of extension obtained from the trilateration and that obtained from the focal mechanism solution is 9° ± 11°, well within the uncertainties. The observed strain rate allows us to make a crude estimate of the recurrence time for earthquakes like the 1959 event. *Savage and Hastie* [1966] found that the vertical deformation could best be fit by a model with 10 m of dip slip implying a horizontal extension during the earthquake of about 6 m. Assuming that the Hebgen net spans the total zone of deformation and that the extensional strain is uniform across the net, the 0.2 μstrain/yr rate represents an extension of about 6 mm/yr across the faulted zone. At this rate, about 1000 years would be required to accumulate strain for a Hebgen Lake type event. This interval of course assumes that the strain rate is constant at all stages of the strain accumulation cycle. Focal mechanism solutions obtained for the Yellowstone Park–Hebgen Lake region by *Trimble and Smith* [1975] indicate a complex stress pattern over the region, but the predominant solution is one with a north-south tensional axis. The area covered by the trilateration net is shown with focal plane solutions of *Trimble and Smith* [1975], *Smith and Sbar*

[1974], and *Dewey et al.* [1972] superposed in Figure 5. The trilateration data are qualitatively in agreement with the seismic record.

The situation at Ogden, Utah, is less clear. This net is located on the boundary of the Basin and Range province, an area produced by late Cenozoic extension and presently subjected to WNW-ESE extension [*Thompson and Burke*, 1974]. The Wasatch mountains form the eastern boundary of this province, and the Ogden net crosses the Wasatch fault along the western front of these mountains. At Ogden the deformation is primarily compression at a rate of 0.17 ± 0.02 μstrain/yr in the direction N73°E ± 10°, contrary to the extension expected across a major normal fault. The Ogden network does span the Wasatch fault, and we have no explanation for the apparently reversed strain field.

The Socorro network spans the Rio Grande rift, a possible site of east-west spreading [*Chapin and Seager*, 1975]. We have observed only a minor amount of strain accumulating near Socorro, and the observations offer no support for east-west spreading. The best interpretation of the observations is in terms of a dilatation of −0.14 ± 0.04 μstrain/yr with no significant shear strain. We regard the observed strain rate at Socorro as only marginally significant, and we hesitate to attach much significance to the observed rate. What is significant is the absence of observable east-west spreading. *Woodward* [1977] has estimated the extension rate across the Rio Grande rift near Albuquerque as only 0.3 mm/yr averaged over the past 26 m.y. Such a low rate of spreading would be consistent with our observations.

Reilinger and Oliver [1976], in comparing leveling from the 1911–1912 period with repeat leveling in the 1950–1952 period, have detected a 240-mm uplift centered apparently about 23 km north of Socorro, which must have occurred in the 40-year interval. They suggested that this uplift might be due to magma intrusion in a disc-shaped chamber at a depth of about 18 km. There are two possible interpretations of the uplift observed over a 40-year period. One is that the deformation occurred at a uniform rate over the time spanned by the surveys. A second possibility is that the uplift occurred during one or several episodes over a shorter time interval, as, for example, the southern California uplift of 1959–1974 [*Castle et al.*, 1976]. We have used a model of *Dieterich and Decker* [1975] to estimate the horizontal deformation that would occur as a result of a pressure increase in a disc-shaped magma chamber of thickness 0.9 km and radius 18 km buried at a depth of 18 km, the same model that *Reilinger and Oliver* [1976] used in modeling the vertical movement. The Socorro Geodolite net is well situated for testing this model, since it covers the south half of the uplift out to a distance at which the displacement field is changing only very slightly with increasing radial distance. The disc-shaped magma chamber used by *Reilinger and Oliver* [1976] produces the least amount horizontal deformation of all the shapes studied by *Dieterich and Decker* [1975]. The maximum horizontal displacement is only about 15% of the maximum vertical displacement. Since *Reilinger and Oliver* [1976] find an uplift rate of 6.1 mm/yr, horizontal displacements would be of the order of 1 mm/yr. Table 2 compares the model prediction with the observed rates. The predicted deformation on all lines is within the uncertainty in the observations, so no single line is inconsistent with the model. However, the overall effect of the observed changes is a slight negative dilatation, while the overall effect predicted by the model is a slight positive dilatation. Other shapes for the magma chamber given by *Dieterich and Decker* [1975] produce an even greater areal increase. The Geodolite data make it unlikely that the uplift observed between 1911 and 1951 occurred at a uniform rate which persisted into the 1970's.

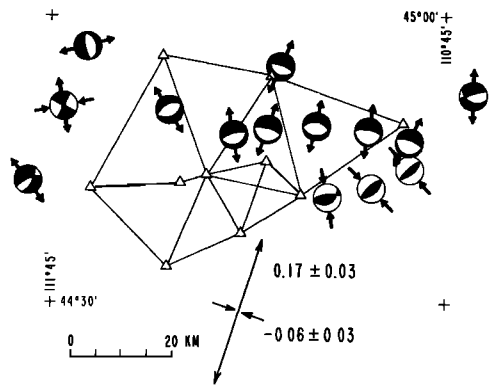

Fig. 5. Diagram of the Hebgen net showing focal plane solutions [from *Trimble and Smith*, 1975]. Triangles indicate station locations, and connecting lines indicate those lines that are measured. Arrows on focal spheres indicate horizontal projection of tensional and compressional axes. Arrows at bottom center indicate principal strain axes from trilateration data, labeled in microstrains per year.

Strain Accumulation Rates in California

Seventeen networks in California have been analyzed to determine strain accumulation rates (Figure 3 and 4). All but two are located along the San Andreas fault system. The exceptions are a net on the Garlock fault east of Ridgecrest, California, and a net across the San Gabriel fault at San Fernando. We discuss the nets consecutively from north to south, each net being identified by its name and by the latitude of its projection on the main strand of the San Andreas fault along the direction N50°E (normal to fault).

Geyser, 38.5°N. This net consists of 32 lines, most of which have been surveyed four times between October 1972 and October 1977. It is located about 50 km east of the San Andreas fault and spans the Rogers Creek–Healdsburg fault zone and the Geyser Basin geothermal area (Figure 3). The strain rate components obtained in this area are listed in Table 1. The dilatation, $\dot{\Delta} = -0.13 \pm 0.04$ μstrain/yr, is significant, and there is a significant amount of shear present in the strain field. The shear is $\dot{\gamma} = 0.48 \pm 0.05$ μstrain/yr right lateral engineering shear across a plane with bearing ψ = N31°W

TABLE 2. Average Rate of Change of Line Length Observed and Rate Predicted by Model of *Reilinger and Oliver* [1976]

Line	Observed, mm/yr	Model, mm/yr
Polvadera-Mines	−0.3 ± 1.4	1.0
Polvadera-Granite	−1.6 ± 1.8	0.3
Polvadera-Canas	−0.0 ± 1.8	2.1
Polvadera-Alamillo	−0.4 ± 1.6	1.8
Mines-Granite	−2.4 ± 2.0	1.1
Mines-Chupadera	−1.9 ± 2.1	−0.3
Mines-Canas	−0.9 ± 1.9	1.5
Mines-Campana	−4.7 ± 2.7	0.3
Mines-Alamillo	−1.6 ± 1.7	1.6
Holcomb-Canas	−1.0 ± 1.6	−0.4
Chupadera-Canas	−3.5 ± 2.6	0.5
Chupadera-Campana	0.2 ± 1.9	0.6
Canas-Campana	−1.2 ± 2.1	−0.2
Canas-Alamillo	−1.3 ± 1.4	0.7

Uncertainty quoted is 1 standard deviation. Observed data are from the Socorro Geodolite net.

± 3°. This is somewhat surprising in view of the net's location, spanning an active geothermal area. Several stations in the net are located in or very near the geothermal field and are obviously being affected by it. In spite of this the overall deformation is right lateral shear across a plane parallel to the local strike of the Healdsburg fault 15 km to the west.

Santa Rosa, 38.3°N. The Santa Rosa net is located 50 km south of the Geyser net. It consists of 13 lines observed three times between March 1972 and March 1976. The strain components obtained in the area are $\dot{\Delta} = 0.01 \pm 0.10$ μstrain/yr, $\dot{\gamma} = 0.33 \pm 0.10$ μstrain/yr, and ψ = N43°W ± 9°. The field is completely shear with no dilatation. The direction of maximum right lateral shear agrees very well with the N40°W trend of the Healdsburg–Rogers Creek faults, which the net spans, and the San Andreas fault 30 km to the west.

Point Reyes, 38.1°N. This is a small-diameter net of 17 lines located across the San Andreas fault near Point Reyes National Seashore. Although a few lines were first observed in March 1972, most of the lines have only been observed twice, once in October 1974 and once in April 1976. The strain rates obtained for this net are $\dot{\Delta} = -0.32 \pm 0.25$ μstrain/yr, $\dot{\gamma} = 0.73 \pm 0.25$ μstrain/yr, and ψ = N35°W ± 8°. The larger standard deviations for this net are a result of the short time period, only 1.5 years, spanned by the net and the short average line length, only 8 km. The only significant aspect of the strain field is the shear, which agrees in direction with the local strike of the San Andreas fault (N40°W). Although the rate of shear straining appears high in comparison to other areas along the fault, the standard deviation is so large that at the 95% confidence limit the Point Reyes shear rate does not differ significantly from more typical values of about 0.2 μstrain/yr.

Thatcher [1975*b*] has examined triangulation data covering the same area as the Santa Rosa and Point Reyes nets. From a comparison of triangulation done in 1930, 1938, and 1961 he found engineering shear strain accumulation at an annual rate of $\dot{\gamma} = 0.38 \pm 0.10$ μstrain/yr and a direction of N43°W ± 8°. The triangulation data in the vicinity of Point Reyes are noisier than at Santa Rosa, and since the trilateration is also noisy at Point Reyes, a direct comparison is probably not meaningful. However, the rate obtained above for Santa Rosa (0.33 ± 0.10 μstrain/yr, N43°W + 9°) agrees with the average rate that *Thatcher* [1975*b*] obtained from all the Point Reyes Petaluma triangulation data.

Napa, 38.0°N. The Napa network, consisting of 13 lines located in the vicinity of Napa, California, was originally surveyed in March 1970 by the City of Napa. The actual field work was done by a private surveying firm using procedures similar to those employed by the U.S. Geological Survey. In April 1976 the lines were reobserved both by the USGS and by the CDMG. The USGS observations were made using the techniques described above. The CDMG observations were made by the same surveyor who had made the original observations. The principal difference is that the city and CDMG surveys employed a model 8 Geodimeter rather than a Geodolite. The agreement between the two 1976 surveys was excellent. This is the only net to be discussed for which observations other than Geodolite are used. The strain field resulting from a comparison of the 1970 and 1976 surveys has components $\dot{\Delta} = -0.21 \pm 0.03$ μstrain/yr, $\dot{\gamma} = 0.17 \pm 0.03$ μstrain/yr, and ψ = N8°W ± 5°. Both the shear and the dilatation differ significantly from zero. The Napa net is located 50 km east of the San Andreas fault and is the most distant net to indicate a significant amount of shear. The orientation of the shear is more northerly than the San Andreas, in closer agreement with the strike of the Green Valley fault located to the east of Napa. The Green Valley fault strikes N20°W and shows evidence of Quaternary, but no historic, activity [*Jennings*, 1975].

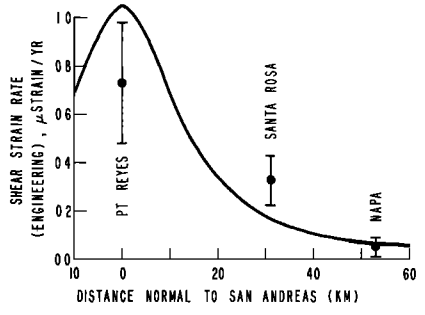

Fig. 6. Attenuation of strain rate with distance normal to San Andreas fault. Points indicate observed strain rates. Bars indicate ±1 standard deviation. Curve is least squares best fit to three points, assuming (6) of text describes attenuation. For curve, $\dot{b}$ = 46 ± 11 mm/yr, and D = 14 ± 5 km.

The three nets, Point Reyes, Santa Rosa, and Napa, are located on nearly the same perpendicular to the San Andreas fault. If we assume that strain accumulation across this entire region is a result of slip at depth on the San Andreas fault, then variations in the rate of strain accumulation provide some constraints on the rate of slip and the depth to the slipping zone. We take a simple two-dimensional model of a vertical strike slip fault, locked from the surface to a depth D and below D slipping uniformly at rate $\dot{b}$ [*Savage and Burford*, 1973]. The relation between the shear strain rate observed at the surface and the depth and slip rate is

$$\dot{\gamma}(y) = \dot{b}/[\pi D(1 + y^2/D^2)] \quad (6)$$

where $\dot{\gamma}(y)$ is the engineering shear strain rate parallel to the fault strike at a distance y from the fault trace. The observations at Point Reyes, Santa Rosa, and Napa allow us to estimate $\dot{b}$ and D. For this purpose we are interested only in the component of shear parallel to the San Andreas fault. At Point Reyes and Santa Rosa, essentially all of the shear is parallel to the San Andreas. At Napa the shear parallel to the San Andreas fault is only 0.11 ± 0.03 μstrain/yr. Thus the Napa data serve mainly to limit the distance to which the strain imposed by the San Andreas fault is detected. The data for these three nets are shown in Figure 6, as well as a least squares fit to the data assuming the strain distribution is governed by (6). The observations were weighted by the inverse square of the standard deviations shown in Figure 6. Strain rates for these nets imply a slip rate of 46 ± 11 mm/yr below a depth 14 ± 5 km. The slip rate agrees with either the relative plate motion rate (55 mm/yr) determined by *Atwater and Molnar* [1973] or the 32-mm/yr slip rate determined along the creeping section to the south of Hollister [*Savage and Burford*, 1973]. *Thatcher* [1975*a*] estimated that coseismic slip during the 1906 earthquake extended to a depth of 10 km. That estimate is reasonably consistent with the 14 km determined here as the depth below which slip is continuous and aseismic. The slip rate and depth determined from these data are consistent with other estimates, but the data are not adequate to refine previous estimates. It is likely that the strain rate at Napa and Santa Rosa is in part due to the Rogers Creek and Green Valley faults, in which case a calculation of this type is an oversimplification.

San Francisco Bay, 38.0°–37.0°N. The San Francisco Bay (Figure 7) net consists of 35 lines which have been observed since 1970. The number of observations of each line varies greatly. Some have only two observations, and one has been observed 17 times between 1972 and 1975. The net covers a larger area than most nets, and the density of coverage is less. The area spanned is tectonically complex, containing three major faults (Figure 7). Large earthquakes in the bay area occurred in 1838 and 1906 on the San Andreas and in 1836 and 1868 on the Hayward fault [*Richter*, 1958, p. 473]. Fault creep occurs on the Hayward fault at a rate of about 6 mm/year [*Radbruch*, 1968], and unpublished trilateration data indicate shallow slip on the Calaveras fault at a rate of 6 mm/yr at Calaveras reservoir. The existence of fault creep in this area complicates the analysis, since the strain is inhomogeneous. However, the creep rates are so low in comparison to the plate motion or the fault creep rate farther south that their influence on the average strain rate across the net is likely to be minimal. The strain field determined by least squares fit to the bay net data has components $\dot{\Delta} = -0.16 \pm 0.02$ μstrain/yr, $\dot{\gamma} = 0.47 \pm 0.02$ μstrain/yr, and $\psi = N27°W \pm 2°$. The San Andreas, Hayward, and Calaveras faults strike in slightly different directions: N37°W, N40°W, and N25°W, respectively. The plane of maximum shear strikes significantly more north than the San Andreas or Hayward faults. The bay net spans a large area, and this raises the question of whether the assumption of a uniform strain field across the whole area is valid. One way to test this is to look at various subsets of the data by calculating strain from just the lines in a smaller area. Strain fields were computed from just the lines on the east side of the bay covering the Calaveras and Hayward faults, from just the lines on the west side of the bay covering the San Andreas, and from those lines to the south of the bay. Strain rates determined in this way are given in Table 3. In general, the agreement between the various parts of the area is good, but numerous differences significant at the 95% confidence level are apparent. The high rate of shear straining in the South Bay is undoubtedly a result of creep on the Calaveras fault rather than of strain accumulation. Both the East Bay and the South Bay data sets show a negative dilatation rate of about 0.1 μstrain/yr, while for the West Bay the rate is 3 times as high. Finally, the azimuth of the plane of maximum shear varies from west to east in a manner quite consistent with the strike of the corresponding fault. That is, in the West Bay the strike of the plane of maximum shear and the San Andreas fault both strike significantly more west than the East Bay data and the Calaveras fault.

TABLE 3. Strain Rates Determined From Various Subsets of the Bay Net Data

Area Included	$\dot{\Delta}$, μstrain/yr	$\dot{\gamma}$, μstrain/yr	ψ
All data	-0.16 ± 0.02	0.47 ± 0.02	N27°W ± 2°
East Bay	-0.08 ± 0.03	0.38 ± 0.04	N26°W ± 3°
West Bay	-0.27 ± 0.04	0.48 ± 0.04	N36°W ± 4°
South Bay	-0.09 ± 0.04	0.73 ± 0.04	N26°W ± 2°

Parameter $\dot{\Delta}$ is dilatation rate; $\dot{\gamma}$ is shear rate (engineering); and ψ is bearing of plane of maximum right lateral shear.

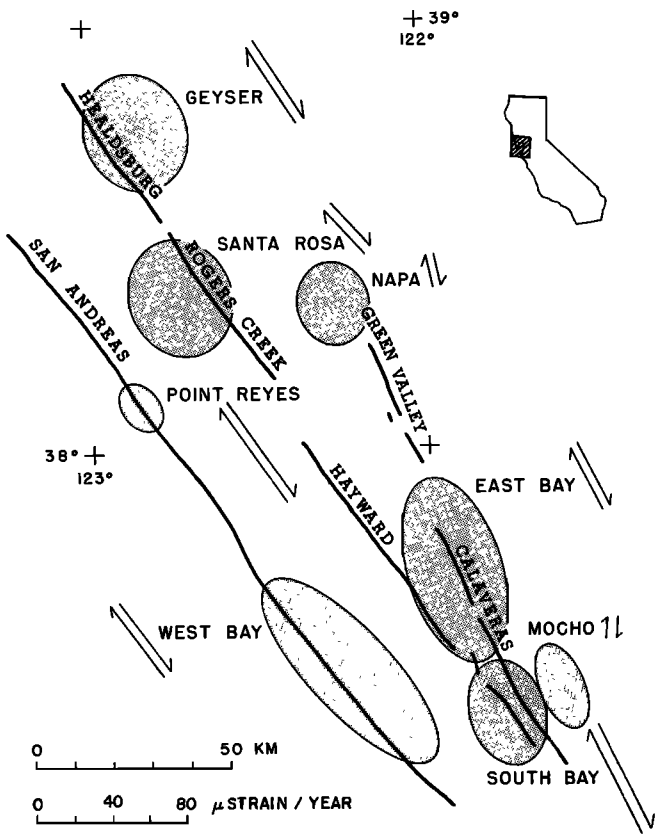

Fig. 7. Schematic illustration of relation between trilateration nets and faults from San Francisco Bay area north. Shaded area is approximately the region spanned by the net. The arrows indicate direction and magnitude of maximum right lateral shear. Numerical values are given in the text and Table 3.

There are three possible sources for the discrepancy in the direction of shear on the two sides of the bay. The first is noise; the difference is 10° ± 5° and thus right at the 2 standard deviation confidence limit. This explanation seems unlikely; surveys on both sides of the bay cover quite a number of years. Additional data will probably not greatly affect the difference. A second possible source of the difference is that the driving stresses vary over this distance, and the strain difference is a reflection of current stress differences. This model requires a locally applied driving mechanism, for example, basal shears at the base of the lithosphere with a discontinuity beneath the bay. The required discontinuity would have to be quite sharp. How sharp would be a function of the effective plate thickness and properties. This model is not very attractive because of the problems involved in creating variations in the driving stress over such short distances. The third possible explanation is that the driving stress is uniform but that deformation is constrained by the existing fault system. This model requires some slip at depth on both the San Andreas and Calaveras faults or at least some flow or plastic behavior localized to the faults. If the faults were completely locked, the strain field would be uniform across the region.

The most likely explanation of the difference in direction of shear appears to be aseismic slip at depth on both the San Andreas and Calaveras faults. An estimate of the maximum depth to the top of the slipping zone can be obtained from the separation of the two faults, utilizing the fact that the strain fields generated by the two faults can be resolved. If the slipping zone were very deep, the surface strain fields would merge, and a distinct shear direction between the East Bay and West Bay would not be observed. From Figure 6 or (6) it is apparent that the strain rate falls to one-half its maximum value at a distance D, the thickness of the locked zone. In Figure 8, (6) has been used to illustrate, in convenient form, the relation between separation of two nearby strike slip faults

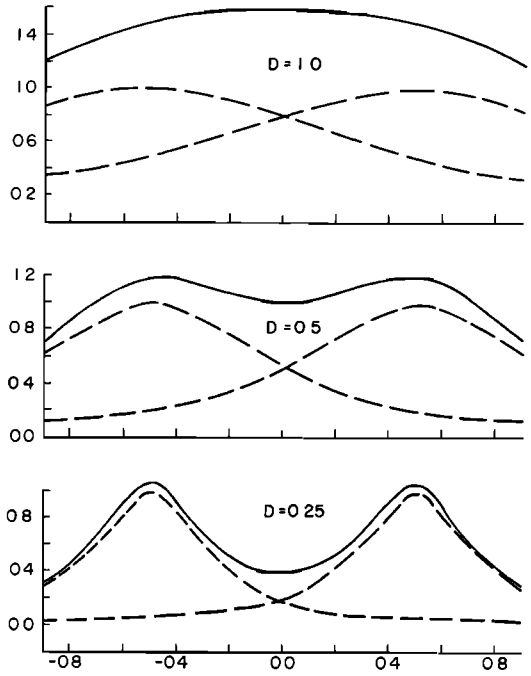

Fig. 8. Illustration of the superposition of the strain fields due to slip at depth on two nearby strike slip faults. In all three cases the faults are located at −0.5 and +0.5. Dashed lines indicate the strain at the surface due to slip on the individual faults. The solid curve is the sum of the two dashed curves in each case. D gives the distance to the top of the slipping zone in units of the fault separation.

and the depth to the top of the slipping zone. From Figure 8 it is apparent that if the thickness D of the locked zone is equal to the fault separation y_0, the strain fields merge completely. If $D = \frac{1}{2}y_0$, the two individual strain fields are just resolvable, and if $D < \frac{1}{2}y_0$, the two fields are well resolved. Figure 8 was calculated for an idealized model of two parallel strike slip faults with the slip rate and depth of locking the same on both faults. We want to apply it to two nonparallel faults for which the observed difference is the direction of shear and not the rate. Thus Figure 8 does not strictly apply to the case we are discussing, but nevertheless, it is useful for estimating the depth of locking. In the bay area the separation between the San Andreas and Calaveras faults is about 45 km. Since we can resolve the difference in strain direction, the depth of locking must be at most $\frac{1}{2}y_0$ = 22 km and probably is $\frac{1}{2}y_0$ = 11 km or less. This result is consistent with the evidence that it was only the upper 10 km of the San Andreas which ruptured in 1906 [*Thatcher*, 1975*a*]. Below 10 km the motion occurs continuously and aseismically. This model is indicated schematically in Figure 9.

We suggest that slip is occurring at depth on both the San Andreas and Calaveras faults. Thus we disagree with the conclusion of *Thatcher* [1975*b*] that before 1940, slip took place on the San Andreas and since 1940 it has transferred to the Hayward-Calaveras. Thatcher's conclusions were based on triangulation, covering the periods 1907–1922, 1922–1948, and 1951–1963. For the first two periods he obtained shear strain directions of N41°W and N36°W. For the third period he obtained a direction of N18°W. Thatcher interpreted these data as the consequence of a transfer of slip at depth from the San Andreas to the Hayward-Calaveras faults. A more likely explanation is that the difference is due to the different areas covered by the data. The first two points in his Figure 4, corresponding to the time periods 1907–1922 and 1922–1948, were obtained from the Primary arc triangulation data. This net covers a large section of the fault and averages strain over a large area. This net covers all three fault systems. The third point in Thatcher's Figure 4 comes from the Hayward net data. This net covers all these faults again, but most of the net is in the East Bay, and thus strain along the Hayward-Calaveras had more effect on the solution than strain along the San Andreas. Only one station out of a total of 20 stations is located west of the San Andreas fault. Thus the change in azimuth indicated by *Thatcher* [1975*b*, Figure 4] is most likely a reflection of a spatial difference in strain accumulation rather than a temporal difference. With this interpretation his data agree with ours quite well. Both indicate shear across an azimuth of about N36°W on the San Andreas fault and N20°W on the Hayward-Calaveras faults. The strain rates obtained by us for the West Bay (Table 3) agree reasonably well with the 1907–1948 rates of shear straining obtained by Thatcher, but the East Bay rate is significantly lower than the 1951–1963 rate he obtained. (This paper, $\dot{\gamma}$ = 0.38 ± 0.04 μstrain/yr; *Thatcher* [1975*b*], $\dot{\gamma}$ = 0.72 ± 0.13 μstrain/yr.)

Mocho, 37.2°N. The Mocho net consists of 12 lines located to the east of Mount Hamilton near San Francisco Bay (Figure 3). Most of these lines have been observed three times, in June 1973, in December 1975, and in July 1978. As Figure 3 indicates, the strain field contains both shear and dilational components. The strain components are $\dot{\Delta}$ = −0.32 ± 0.05 μstrain/yr, $\dot{\gamma}$ = 0.13 ± 0.06 μstrain/yr, and ψ = N7°E ± 12°. The dilatation is well above the noise level and is not likely to be entirely the result of random errors. In addition to the dilatation the strain field at Mocho has a large shear component. The direction of shear is inconsistent with a San Andreas fault type strain field. The shear rate is $\dot{\gamma}$ = 0.13 ± 0.06 μstrain/yr either left lateral across a plane striking N83°W ± 12° or right lateral across a plane striking N7°E ± 12°. This net is the only net studied along the San Andreas fault for which the strain field was inconsistent with right lateral strain accumulation parallel to the San Andreas fault. The net does not span any of the three active fault zones. It is located just east of the bay net, where the shear strain rate is 0.4 μstrain/yr, and parallel to the NW-SE trending faults. More detailed analysis of the data shows that it is the first survey which is anomalous. Between 1975 and 1978 no significant changes occurred; 75% of the strain occurred between 1973 and 1975 and over this shorter time period was even more anomalous than the average rate would indicate. We have no

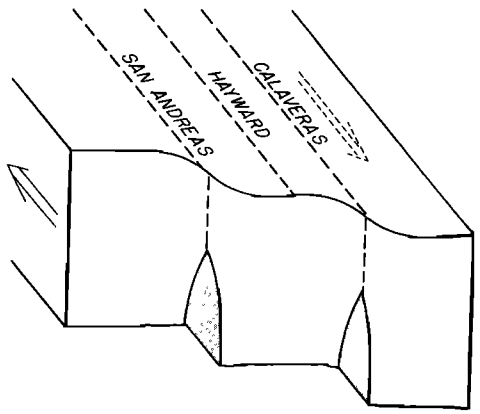

Fig. 9. Schematic model of faults in San Francisco Bay. Slip at depth occurs on two faults resulting in strain accumulation across the entire region. Fault creep on the Hayward and Calaveras faults relieves stress to a shallow depth. Periodically, the stress exceeds some critical level and ruptures through to the surface on one of the traces.

reason to suspect the first survey and also no suggestion of a tectonic origin for the change.

Pajaro, 37.0°N. The Pajaro net consists of 12 lines in the area west of the San Andreas fault between Gilroy, San Juan Buatista, and Monterey Bay (Figure 3). Strain components obtained in this area are $\dot{\Delta} = -0.34 \pm 0.06$ μstrain/yr, $\dot{\gamma} = 0.25 \pm 0.06$ μstrain/yr, and ψ = N49°W ± 80. These values are typical of rates observed elsewhere along the fault, although the direction of shear is more westerly than for other nets in northern California.

Hollister, 36.9°N. This net consists of a small subset of the lines in the complete Hollister net [*Savage et al.*, 1976]. The lines included in this study all lie to the east of the Calaveras fault east and north of the town of Hollister, California. No fault-crossing lines were included in this analysis. The net was surveyed annually between 1971 and 1978. The strain components are well determined because of this long time period. The observed deformation is $\dot{\Delta} = +0.05 \pm 0.04$ μstrain/yr, $\dot{\gamma} = 0.31 \pm 0.04$ μstrain/yr, and ψ = N60°W ± 4°.

Since the strike of the Calaveras near Hollister is N29°W and the strike of the San Andreas is N48°W, the shear observed is significantly more westerly than either of these. No dilatation was observed for this net. The Pajaro and Hollister data indicate that a significant amount of strain is accumulating near the end of the creeping section of the fault. The Hollister net has been discussed in detail by *King et al.* [1978].

Gavilan, 36.8°N. The Gavilan net is a small-diameter net of 19 lines, each observed 5 times between 1970 and 1975. Because the average line length is only 3 km and the uncertainty in strain determinations goes up rapidly for short lines (Figure 1), this net is not very sensitive to strain accumulation. This net is one of several small-aperture nets located near the fault in north central California. The others all had standard deviations greater than 0.2 μstrain/yr, too large to be included in this study. The Gavilan net is located near San Juan Bautista and on the west side of the San Andreas Fault. The deformation is not significant at the 2 standard deviation level: $\dot{\Delta} = -0.24 \pm 0.13$ μstrain/yr, $\dot{\gamma} = 0.22 \pm 0.14$ μstrain/yr, and ψ = N17°W ± 18°.

Los Padres, 35.1°–34.8°N. The Los Padres net is located to the southwest of the San Andreas fault in the Transverse Ranges near the south end of the Carrizo Plains. Deformation observed is $\dot{\Delta} = -0.27 \pm 0.03$ μstrain/yr, $\dot{\gamma} = 0.23 \pm 0.03$ μstrain/yr, and ψ = N48°W ± 5°. North of Los Padres net the San Andreas fault strikes N40°W and to the southeast, N75°W. Shear in the Los Padres net tends to be parallel to the fault in the Carrizo Plains to the north rather than to the fault along the 'big bend' to the southeast.

Tehachapi, 34.8°–34.5°N. The Tehachapi net covers a large area east of the San Andreas fault near the junction of the San Andreas and Garlock faults. Deformation here is very similar to that for the Los Padres Net: $\dot{\Delta} = -0.24 \pm 0.03$ μstrain/yr, $\dot{\gamma} = 0.26 \pm 0.04$ μstrain/yr, and ψ = N59°W ± 4°. The most significant difference between the deformation in the Los Padres net and in the Tehachapi net is the direction of the plane of maximum shear. Here it is more nearly parallel to the big bend section of the San Andreas fault.

Palmdale, 34.6°N. This net consists of 36 lines, mostly short, crossing the San Andreas near Palmdale, California. Deformation here has been discussed by *Prescott and Savage* [1976]. The most recent estimate of the strain rate is $\dot{\Delta} = -0.18 \pm 0.04$ μstrain/yr, $\dot{\gamma} = 0.34 \pm 0.04$ μstrain/yr, and ψ = N57°W ± 4°. The shear is parallel to the local azimuth of the San Andreas, N65°W, and appears to be accumulating at a rate that has not varied since 1932.

San Fernando, 34.6°N. The San Fernando net was first observed following the 1971 San Fernando earthquake. It was also observed in 1973 and 1977. The net consists of 22 lines with lengths of 5–10 km. It crosses the thrust faults which ruptured during the earthquake but lies entirely south of the San Gabriel fault. The strain rate data are $\dot{\Delta} = -0.44 \pm 0.06$ μstrain/yr, $\dot{\gamma} = 0.42 \pm 0.06$ μstrain/yr, and ψ = N36°W ± 4°. The earliest data used in this determination are those of August 1971, 7 months after the earthquake; thus the data are probably not contaminated by postseismic effects. *Savage and Church* [1975] concluded that any afterslip must have preceded the August 1971 survey.

Cajon, 34.3°N. The Cajon net is located north of San Bernardino, California, across the junction of the San Andreas, San Jacinto, and San Gabriel fault zones. The observed strain field is $\dot{\Delta} = -0.33 \pm 0.10$ μstrain/yr, $\dot{\gamma} = 0.40 \pm 0.10$ μstrain/yr, and ψ = N46°W ± 10°. There are 30 lines in the Cajon net, but most have only been surveyed twice, and many are shorter than is ideal for strain determinations.

Anza, 34.2°–33.7°N. This net consists of a large number of lines and covers a very large area. On the west it extends across the Elsinore fault along the Santa Ana mountains. On the north it extends to the San Bernardino Valley and on the east to the San Andreas fault north of the Salton Sea. Best coverage afforded by the net is across the seismically active San Jacinto fault zone. A small subset of this net located in the immediate vicinity of the San Jacinto fault zone was examined by us in an earlier paper [*Savage and Prescott*, 1976]. In that study we found that the deformation was right lateral shear parallel to the San Jacinto at a rate of $\dot{\gamma} = 0.4 \pm 0.1$ μstrain/yr. In contrast to those 6 lines close to the San Jacinto, the 60 lines of the complete Anza net indicate a somewhat slower rate of strain accumulation. The shear and dilatation rates obtained are $\dot{\Delta} = -0.31 \pm 0.03$ μstrain/yr, $\dot{\gamma} = 0.23 \pm 0.03$ μstrain/yr, and ψ = N47°W ± 5°. As was pointed out in our earlier paper, the near-fault strain determination implies a ratio of slip rate to the depth of the locked zone of about 1.2×10^{-6} year using a simple model of slip at depth beneath a locked zone.

Salton, 33.7°–32.7°N. The Salton net spans the San Andreas and associated faults in Imperial Valley and around the Salton Sea. It is a broad net containing 48 lines. The observed deformation consists of $\dot{\Delta} = -0.26 \pm 0.02$ μstrain/yr, $\dot{\gamma} = 0.34 \pm 0.02$ μstrain/yr, and ψ = N47°W ± 2°. The faults around the Salton Sea show a great deal of variation in strike when examined in detail, but the overall strike is roughly N40°W, consistent with the shear direction obtained from the trilateration data. This net is discussed in more detail by *Savage et al.* [1979].

Garlock. The other net in California for which data are available covers about 150 km along the Garlock fault from south of Ridgecrest, California, to the southern tip of Death Valley. It consists of 21 lines. The strain rate data are $\dot{\Delta} = -0.17 \pm 0.04$ μstrain/yr, $\dot{\gamma} = 0.16 \pm 0.04$ μstrain yr, and ψ = N64°E ± 8° for left lateral shear. The data are consistent with left lateral shear along the Garlock fault. The rate is about half the typical rate for San Andreas nets. The Garlock fault strikes N70°E in the region covered by this net.

DISCUSSION

Figures 10–12 summarize the results obtained along the San Andreas fault in California. Figure 10 is a plot of the maximum shear $\dot{\gamma}$. The data in Southern California all indicate a rate of 0.2–0.4 μstrain/yr. The data in northern California are much more variable. Clearly, part of this greater variability is due to noise. The Point Reyes (38.1°N) and Gavilan (36.8°N)

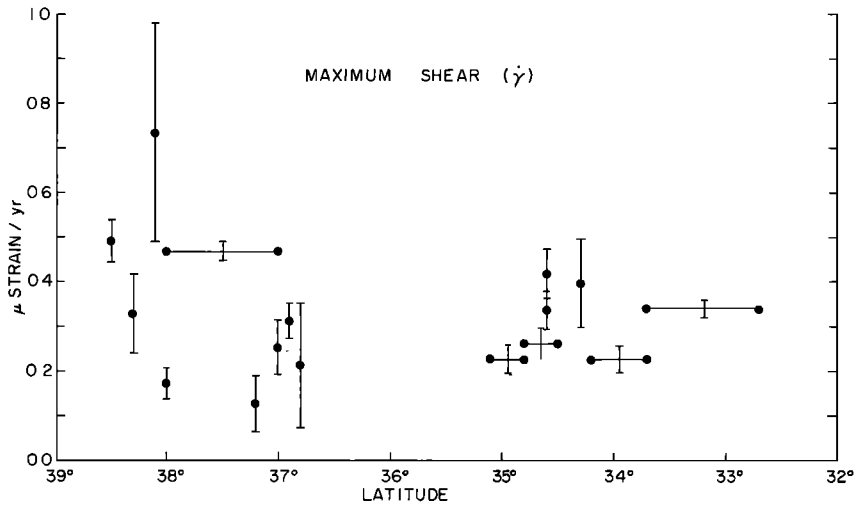

Fig. 10. Variation of shear strain $\dot{\gamma}$ with position along the San Andreas fault system in California. Error bars (vertical lines) indicate ±1 standard deviation. A horizontal line connecting two dots indicates the range covered by a single net.

nets are both small nets with large standard deviations. Of the remaining nets in northern California, all but two (that is, the other five) have shear strain rates between 0.2 and 0.5 μstrain/yr. The two exceptions are Napa (38.0°) and Mocho (37.2°). Both of these nets have relatively low rates of strain accumulation. Figure 7 summarizes the relation between the faults and nets in northern California. As discussed above, the bay net data indicate that slip at depth is occurring on both the San Andreas and Calaveras faults. The absence of any significant shear in the Napa data implies that north of the bay area, slip at depth on the Calaveras fault terminates. Since both Santa Rosa and Geyser are showing appreciable shear, the slip presumably is transferred to the Rogers Creek–Healdsburg faults. Not much can be said about slip at depth on the Hayward fault in the bay area. There is strain accumulation near the San Andreas fault throughout this area as evidenced by the Point Reyes and West Bay data. A priori these facts could either be interpreted as the result of slip at depth beneath a fairly deep locked section leading to a very broad zone of straining or as a consequence of slip at depth on both the San Andreas and Hayward–Rogers Creek–Healdsburg faults. In the first case the depth to the bottom of the locked zone would have to be 50 km or more, equal to the fault spacing. In the second case the depth to the bottom of the locked zone on each fault would have to be 10 km or more. In neither case do the Point Reyes, West Bay, Geyser, Santa Rosa, or East Bay data provide a lower limit estimate of the locking depth. The Napa and Mocho data allow us to discriminate between the two possibilities, one or two slipping zones at depth; and furthermore, the Napa and Mocho data provide a lower estimate of the locking depth. Throughout this discussion we are using the fact that the half-magnitude width of straining due to slip at depth is equal to the locked depth (see Figure 6 for an example). The lower rate of shear strain in the Napa and Mocho nets indicates that they are well off the peak of the strain curve. If there were a single slip zone at depth, which was deep enough to produce nearly constant shear across the area spanned by all five nets listed above, the strain would also have extended to include Mocho and Napa. Since these show little strain, this is not likely, and a more probable explanation is

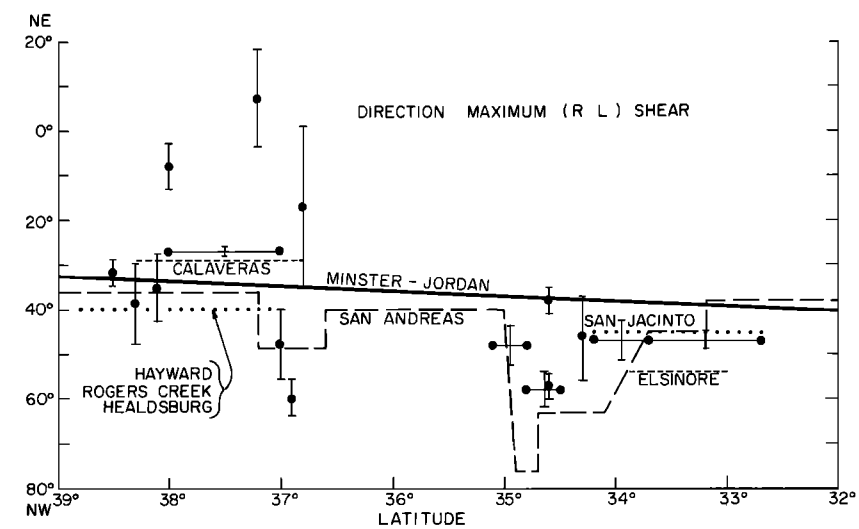

Fig. 11. Variation of direction of maximum shear ψ with position along the San Andreas fault system in California. Error bars (vertical lines) indicate ±1 standard deviation. A horizontal line connecting two dots indicates the range covered by a single net. The long straight line indicates the direction of relative plate motion calculated from the rotation pole of *Minster and Jordan* [1978]. Dotted and dashed lines are directions of fault strike [from *Jennings*, 1975] for various faults within the San Andreas system.

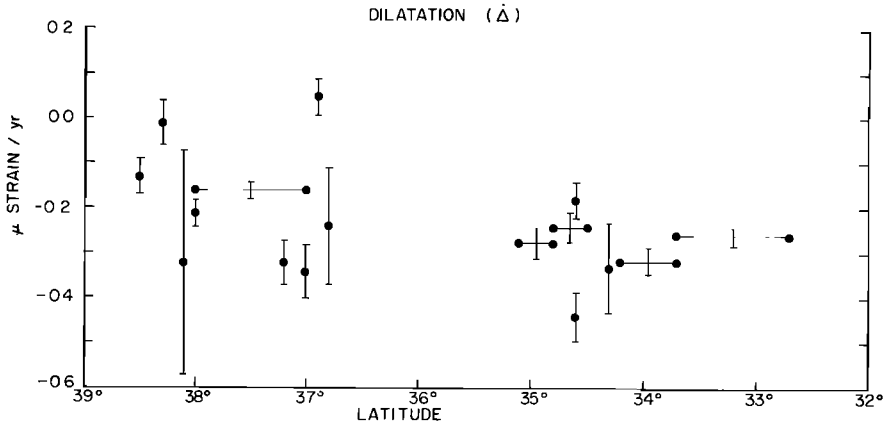

Fig. 12. Variation of dilatational strain $\dot{\Delta}$ with position along the San Andreas fault system in California. Error bars (vertical lines) indicate ±1 standard deviation. A horizontal line connecting two dots indicates the range covered by a single net.

that of two slipping zones, one under the surface trace of the San Andreas and one under the surface trace of the Calaveras–Rogers Creek–Healdsburg faults. It was pointed out in an earlier section that the Napa data restricted slip on the San Andreas fault to below 15 km. The restriction on the Calaveras–Rogers Creek–Healdsburg fault system is even greater, since Napa and Mocho are so much closer to this fault system. On the Calaveras–Rogers Creek–Healdsburg system the depth of locking must be no greater than about 10 km. Note that there is no evidence of a difference in the depth of locking on the two faults; it is only that the geometry of the data provides a tighter control on the eastern fault system than on the San Andreas fault. The Napa and Mocho nets actually place a greater restriction on the width of the zone of strain accumulation than is apparent from Figure 10. It is shown below that the small amount of shear strain at Napa and Mocho shown in Figure 10 is not occurring across the direction of the faults and thus cannot be due to slip at depth on either the San Andreas or Calaveras faults. The shear strain at Napa and Mocho across the direction N33°W is 0.11 ± 0.03 and 0.01 ± 0.05 μstrain/yr, respectively. Hence the strain field due to slip at depth on both the Hayward and San Andreas fault systems is essentially zero at these locations.

In contrast to northern California, shear strain rates in Southern California are more homogeneous (Figure 10). A horizontal line at 0.3 μstrain/yr would fall within 2 standard deviations of six of the seven data points in Southern California. The lone exception is the San Fernando datum (34.6°N). This net spans the San Gabriel fault zone and may be contaminated by the San Fernando earthquake, the only earthquake of magnitude >5.5 to occur near one of these nets in this decade. Consequently, there is no evidence of any variation in the shear strain rate with position along the San Andreas fault system in Southern California. The Garlock net, located 200 km east of the San Andreas fault (Figure 4), has a significantly lower, though nonzero, rate of shear ($\dot{\gamma}$ = 0.16 ± 0.04 μstrain/yr). Although the data presented here are too sparse to infer much detail about strain accumulation in Southern California, it does appear to be a much broader, smoother feature than in northern California. This is not merely an artifact resulting from the fact that more of the Southern California nets are large broad nets. In a detailed analysis of the strain accumulation in the Salton trough, *Savage et al.* [1978] found that along a direction normal to the trend of the faults the shear strain profile was very broad with a maximum on the San Jacinto fault of 0.5 μstrain/yr and a decay to about half this value 20 km west and 60 km east of the San Jacinto fault.

In Figure 11 we have plotted the bearing of the plane across which right lateral shear is maximum. Also shown in Figure 11 are the strikes of the principal strike slip faults in California and the direction of relative plate motion obtained from the solution of *Minster and Jordan* [1978]. Straight sections of a fault plot as horizontal lines, and an abrupt change of fault strike plots as a vertical line. Thus the Carrizo Plains section of the San Andreas is represented by the horizontal dashed line from 38.6°N to 35.0°N. At each end of it are sections with a more westerly strike, the little bend from 37.2°N to 36.6°N and the big bend from 35.0°N to 33.7°N. The local fault strike is generally within 2 standard deviations of the observed shear strain direction. In fact, nets located along the two major deviations from the overall N35°W trend, the big (Hollister, 36.9°N; Pajaro, 37.0°N) and little (Palmdale, 34.6°N; Tehachapi, 34.5°–34.8°N) bends, reflect these changes in trend. There are three exceptions. At Napa (38.0°N), Mocho (37.2°N), and San Fernando (34.6°N) the direction of shear strain is inconsistent with shear stain on nearby faults. It was pointed out earlier that the shear strain rates at Napa and Mocho are quite low; in fact at Mocho the rate is not significantly nonzero. The third exception is San Fernando, which again has previously been identified as anomalous. The Gavilan (36.8°N) data point is too uncertain to contribute anything to the discussion. With these three exceptions the direction of shear strain accumulation is in very good agreement with the local fault strike. North of 37.5°N the direction of the local fault strike and the direction of relative plate motion implied by *Minster and Jordan*'s [1978] relative motion pole position are the same. South of latitude 37.5°N, however, the direction of the faults deviates significantly from the relative motion direction. The direction of shear strain accumulation consistently follows the local faults and ignores the gross plate motion direction.

From Figure 12 it is apparent that the dilatational component of strain is predominantly compressional all along the San Andreas fault in California. There are only two exceptions: at Hollister and at Santa Rosa. All the other locations indicate compression at a rate which averages −0.22 ± 0.12 μstrain/yr. As pointed out by *Frank* [1966], the determination of shear strains from geodetic data is independent of scale control. Errors which affect all lines in proportion to their length will have no effect on observed shear strains.

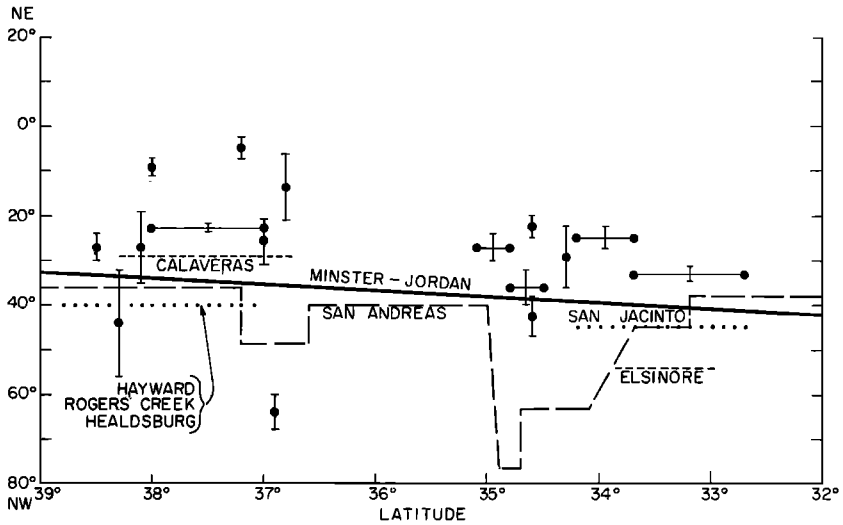

Fig. 13. Variation of direction of shear with position along the San Andreas fault system in California assuming strain field is a pure shear plus a uniaxial strain in direction N55°W. Error bars (vertical lines) indicate ±1 standard deviation. A horizontal line connecting two dots indicates the range covered by a single net. The long straight line indicates the direction of relative plate motion calculated from the rotation pole of *Minster and Jordan* [1978]. Dotted and dashed lines are directions of fault strike [from *Jennings*, 1975] for various faults within the San Andreas system.

Dilatation, on the other hand, is very sensitive to this type of error. As discussed by *Savage et al.* [1978], we have carefully considered possible sources of a systematic error and find that while there is no way to exclude the possibility, it seems unlikely that the observed dilatation is a result of survey errors.

The alternative is that the observed dilatation is of tectonic origin. This requires a mechanism for generating a nearly uniform negative dilatation at nearly every location where strain has been measured in California. The only net in California not shown in Figure 12, the Garlock net, is also undergoing a negative dilatation of -0.17 ± 0.04 μstrain/yr. The fact that the dilatation rate is so similar everywhere in California strongly suggests that all of the observed dilatations have a common origin. *Savage et al.* [1978] discuss a number of sources for this uniform dilatation. In light of its uniformity along the whole length of the San Andreas in California, however, mechanisms associated with the big bend or the 'Palmdale bulge' seem untenable, since these features are relevant only in Southern California. Another possibility is that the Coast Ranges are being squeezed between the Pacific plate and the east-west spreading Basin and Range Province. The following argument, however, demonstrates that this also is an unlikely explanation. Suppose that the strain fields observed along the San Andreas fault system in California arise from a superposition of two strain fields: (1) a nondilatational shear field arising from the northwestward motion of the Pacific plate relative to the North American plate and (2) a uniaxial compression arising from spreading of the Basin and Range province to the east. In this case the dilatational component of the observed strain will result entirely from the uniaxial strain field. The shear will not contribute to the dilatation at all. Hence for this model, Figure 12 can be interpreted as a plot of the magnitude of the uniaxial compression (strain field 2) at various points along the fault. Figures 10 and 11 do not directly give information about strain field 1, the shear. This is because there is also some shear associated with a uniaxial strain. To see what strain field 1 looks like, it would be necessary to correct Figures 10 and 11 to remove the shear part of strain field 2. In general, both the magnitude and direction of the observed strain will differ from shear field 1. Now since a priori we have no idea what the magnitude of the strain field should be, the change in magnitude does not hurt anything. On the other hand, we do have independent evidence for the direction of shear. Since the observed directions agree quite well with surficial fault traces, a mechanism of the sort discussed here is unlikely—it would destroy this agreement. As a concrete example, we have calculated the magnitude and direction of the shear part (strain field 1) assuming that the dilatation arises from a uniaxial strain in the direction N55°W (*Thompson and Burke* [1974], direction of Basin and Range extension). Since compression in this azimuth gives a left lateral shear on the San Andreas fault direction, the magnitudes of the shear plotted in Figure 10 are generally increased. The effect on the direction of shear is harder to visualize. It is shown in Figure 13. A comparison of Figures 11 and 13 reveals that the observed direction of shear (Figure 11) is in much better agreement with either the fault directions or Minster and Jordan's direction than is the shear direction obtained by correcting for a uniaxial strain with a bearing N55°W. The same criticism would apply to any uniaxial strain field except for one at 45° to the fault directions. Uniaxial strain in this direction would affect only the magnitude of the observed shear, not the direction. Consequently, it appears unlikely that the observed dilatation arises from the superposition of a uniaxial strain on the shear due to relative motion between the Pacific and North American plates.

Acknowledgments. Many people have worked on collecting and processing the data upon which this study was based. Pat Yamashita and Karen Wendt deserve special mention for their work in data reduction, and Ken Yamashita, Nick Sanchez, Mike Lisowski, and Gary Hamilton for their work in the field surveys.

REFERENCES

Atwater, T., and P. Molnar, Relative motion of the Pacific and North American plates deduced from sea floor spreading in the Atlantic Indian, and South Pacific ocean, Proceedings of the Conference on Tectonic Problems of the San Andreas, *Stanford Univ. Publ. Univ. Ser. Geol. Sci., 13*, 136–138, 1973.

Castle, R. O., J. P. Church, and M. R. Elliot, Aseismic uplift in southern California, *Science, 192*, 251–253, 1976.

Chapin, C. E., and W. R. Seager, Evolution of the Rio Grande rift in the Socorro and Las Cruces areas, New Mexico, in *Guidebook 26th Field Conference of the New Mexico Geological Society*, pp. 298–321, Albuquerque, N. Mex., 1975.

Dewey, J. W., W. H. Dillinger, J. Taggert, and S. T. Algermissen, A technique for seismic zoning: Analysis of earthquake locations and mechanisms in northern Utah, Wyoming, Idaho, and Montana, in *Proceedings International Conference on Microzonation for Safer Construction in Research and Applications*, vol. 2, pp. 879–894, University of Washington, Seattle, 1972.

Dieterich, J. H., and R. W. Decker, Finite element modeling of surface deformation associated with volcanism, *J. Geophys. Res., 80*, 4094–4102, 1975.

Frank, F. C., Deduction of earth strains from survey data, *Bull. Seismol. Soc. Amer., 56*, 35–42, 1966.

Jaeger, J. C., and N. G. W. Cook, *Fundamentals of Rock Mechanics*, Methuen, London, 1969.

Jennings, C. W., Fault map of California with locations of volcanoes, thermal springs and thermal wells, *Calif. Geol. Data Map Ser., 1*, Calif. Div. Mines and Geol., San Francisco, 1975.

King, N., J. C. Savage, W. H. Prescott, and M. Lisowski, Geodetic measurement of deformation in the vicinity of Hollister, California 1971–1978 (abstract), *Eos Trans. AGU, 59*(12), 1209, 1978.

Minster, J. B., and T. H. Jordan, Present-day plate motions, *J. Geophys. Res., 83*(B11), 5331–5354, 1978.

Myers, W. B., and W. Hamilton, Deformation accompanying the Hebgen Lake earthquake of August 17, 1959, *U.S. Geol. Surv. Prof. Pap., 435*, 55–97, 1964.

Prescott, W. H., An extension of Frank's method for obtaining crustal shear strains from survey data, *Bull. Seismol. Soc. Amer., 66*, 1847–1853, 1976.

Prescott, W. H., and J. C. Savage, Strain accumulation on the San Andreas fault near Palmdale, California, *J. Geophys. Res., 81*, 4901–4908, 1976.

Radbruch, D. H., New evidence for historic fault activity in Alameda, Contra Costa and Santa Clara counties, California, Proceedings of the Conference on Geological Problems of the San Andreas Fault System, *Stanford Univ. Publ. Univ. Ser. Geol. Sci., 11*, 1968.

Reilinger, R., and J. Oliver, Modern uplift associated with a proposed magma body in the vicinity of Socorro, New Mexico, *Geology, 4*, 583–586, 1976.

Richter, C. F., *Elementary Seismology*, W. H. Freeman, San Francisco, 1958.

Rogers, T. H., and R. D. Nason, Active displacement on the Calaveras fault zone at Hollister, California, *Bull. Seismol. Soc. Amer., 61*(2), 399–416, 1971.

Ryall, A., The Hebgen Lake, Montana earthquake of August 18, 1959: *P* waves, *Bull. Seismol. Soc. Amer., 52*, 235–271, 1962.

Savage, J. C., and R. O. Burford, Geodetic determination of relative plate motion in central California, *J. Geophys. Res., 78*, 832–845, 1973.

Savage, J. C., and J. P. Church, Evidence for afterslip on the San Fernando fault, *Bull. Seismol. Soc. Amer., 65*(4), 829–834, 1975.

Savage, J. C., and L. M. Hastie, Surface deformation associated with dip-slip faulting, *J. Geophys. Res., 71*, 4897–4904, 1966.

Savage, J. C., and W. H. Prescott, Precision of Geodolite distance measurements for determining fault movements, *J. Geophys. Res., 78*, 6001–6008, 1973.

Savage, J. C., and W. H. Prescott, Strain accumulation on the San Jacinto fault near Riverside, California, *Bull. Seismol. Soc. Amer. 66*, 1749–1754, 1976.

Savage, J. C., W. T. Kinoshita, and W. H. Prescott, Geodetic determination of strain at the Nevada Test Site following the Handley event, *Bull. Seismol. Soc. Amer., 64*, 115–129, 1974.

Savage, J. C., M. A. Spieth, and W. H. Prescott, Preseismic and coseismic deformation associated with the Hollister, California earthquake of November 28, 1974, *J. Geophys. Res., 81*, 4901–4908, 1976.

Savage, J. C., W. H. Prescott, M. Lisowski, and N. King, Strain in Southern California: Measured uniaxial north-south regional contraction, *Science, 202*, 883–885, 1978.

Savage, J. C., W. H. Prescott, M. Lisowski, and N. King, Deformation across the Salton Trough, California, 1973–1977, *J. Geophys. Res., 84*, 3069, 1979.

Smith, R. B., and M. L. Sbar, Contemporary tectonics and seismicity of the western United States with emphasis on the Intermountain Seismic Belt, *Geol. Soc. Amer. Bull., 85*, 1205–1218, 1974.

Thatcher, W., Strain accumulation and release mechanism of the 1906 San Francisco earthquake, *J. Geophys. Res., 80*, 4862–4872, 1975*a*.

Thatcher, W., Strain accumulation on the northern San Andreas fault zone since 1906, *J. Geophys. Res., 80*, 4873–4880, 1975*b*.

Thompson, G. A., and D. B. Burke, Regional geophysics of the Basin and Range province, *Annu. Rev. Earth Planet. Sci., 2*, 213–238, 1974.

Trimble, A. B., and R. B. Smith, Seismicity and contemporary tectonics of the Hebgen Lake-Yellowstone Park region, *J. Geophys. Res., 80*, 733–741, 1975.

U.S. Department of Commerce, Earthquake History of the United States, *Publ. 41-1*, review edition (through 1970), U.S. Government Printing Office, Washington, D. C., 1973.

Woodward, L. A., Rate of crustal extension across the Rio Grande rift near Albuquerque, New Mexico, *Geology, 5*, 269–272, 1977.

(Received March 1, 1978;
revised March 19, 1979;
accepted March 26, 1979.)